

**ICSO 2016**

**International Conference on Space Optics**

Biarritz, France

18–21 October 2016

*Edited by Bruno Cugny, Nikos Karafolas and Zoran Sodnik*



***Design optimization of fiber amplifiers exposed to high gamma-radiation doses***

*O. de Vries*

*T. Schreiber*

*R. Eberhardt*

*A. Tünnermann*

*et al.*



icso proceedings



## DESIGN OPTIMIZATION OF FIBER AMPLIFIERS EXPOSED TO HIGH GAMMA-RADIATION DOSES

O. de Vries<sup>1</sup>, T. Schreiber<sup>1</sup>, R. Eberhardt<sup>1</sup>, A. Tünnermann<sup>1,2</sup>, M. Windmüller<sup>3</sup>, J. Riedel<sup>3</sup>, M. Rößler<sup>3</sup>, F. Kolb<sup>3</sup>  
<sup>1</sup>Fraunhofer Institute for Applied Optics and Precision Engineering, Albert-Einstein-Str. 7, 07745 Jena,

Germany

<sup>2</sup>Institute of Applied Physics, Abbe Center of Photonics, Friedrich-Schiller-University Jena, Albert-Einstein-Str. 6, Germany

<sup>3</sup>Jena-Optronik GmbH, Otto-Eppenstein-Str. 3, 07745 Jena, Germany

### I. INTRODUCTION

Fiber lasers entered numerous applications due to their high efficiency and superior stability. Er-doped fiber lasers emitting around 1550 nm optical wavelength are capable to produce hundreds of Watts [1] and Millijoule pulse energy [2,3]. However, for space applications those lasers have to fulfill additional requirements set by the harsh environment, typically characterized by large temperature gradients, vibration and shock as well as different kinds of radiation. To meet those requirements, the realization of an all-fiber design and thus, an adjustment-free laser is most beneficial [4,5]. One of the most important aspects for long term operation in space is the influence of ionizing radiation, which typically leads to strong absorptions in active fibers [6,7]. As a result, radiation-resistant fibers are recommended [8,9]. Nevertheless, the performance of fiber amplifiers has to be considered including these radiation-induced absorption losses during mission lifetime.

In this contribution, an experimental as well as a numerical study on an Er-doped single-clad fiber-based pre-amplifier system was conducted. Due to the low seed power and the high gain, the double-pass type setting is most sensitive to the influence of core-size, doping concentration and ionizing radiation. In section II, the performance of five different fibers is experimentally investigated and compared, followed by a numerical study on the impact of radiation-induced gain reduction in section III. The presented results can be conceived as a guideline how to design a low seed power high-gain preamplifier for use in space.

### II. EXPERIMENT: SETUP AND FIBERS BENCHMARK

The harsh environment during space flight missions includes per se a potentially threatening high dose of high-energy radiation. This is the reason why radiation-hardened rare-earth-doped gain fibers are getting more and more attractive for a variety of space-related applications. On the other side, those applications additionally demand a high degree of amplifier performance and compliance towards existing fiber-optical components. Thus, making comparative experiments between standard and radiation-hardened gain fibers within an otherwise identical testbed is an adequate means to evaluate the performance of a space-qualified fiber amplifier, which inherently involves varying splice losses due to differences in core-size and core-NA. For this reason, five commercially available Er-doped single-clad fibers were consecutively implemented in an all-fiber experimental setup shown in Fig. 1. Two of the five fibers have radiation-hardened properties whereas the three remaining standard-type fibers exhibit different parameters to additionally judge the functional impact of core-size and doping concentration (Table 1).

**Table 1** Basic parameters of the tested fibers

fiber #	fiber type	core-diameter ( $\mu\text{m}$ )	peak core-absorption at 1530 nm (dB/m)
1	standard	8	80
2	standard	4	80
3	standard	4	30
4	rad-hard	4	5
5	rad-hard	4	15

Since the 1550-nm ns-pulsed distributed feedback laser seed diode is operated at a pulse repetition frequency reaching from 150 kHz down to 20 kHz the produced seed power is accordingly low (6.2  $\mu\text{W}$  @ 20 kHz). This circumstance makes e.g. a small-core gain fiber with a lower saturation power possibly the better choice for the intended application. The 8-ns long pulses are electronically generated at the seed diode and propagate towards the double-pass amplifier passing through a fiber-optical circulator (CIRC) and wavelength-division-multiplexer (WDM). The amplifier fiber (FuT, fibers under test) is pumped by means of a wavelength-stabilized single-mode laser diode at 976 nm. To increase spectral purity, a fiber Bragg grating (FBG) with 3-nm bandwidth

around the 1550 nm laser emission wavelength is utilized. The residual pump power can be monitored and analyzed using output port OUT-2. Since this fiber amplifier stage is planned as an all-fiber solution, a high level of residual pump has to be avoided to prevent deterioration of the embedding material. The FBG-back-reflected pulse is amplified a second time and guided towards the output port OUT-1 where the main signal performance data can be acquired.

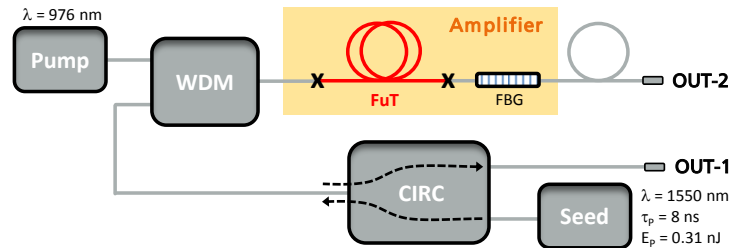


**Figure 1** Schematic of the all-fiber experimental setup used to acquire amplifier performance data for different gain fibers (FuT, fibers under test; FBG, fiber Bragg grating; WDM, wavelength-division-multiplexing; CIRC, optical circulator; OUT-1, main output; OUT-2, output for characterizing the residual emission).

A comprehensive series of tests were performed for each fiber type by systematically varying the parameters of fiber length, pump power and pulse repetition frequency (PRF), which can be reinterpreted as a change in seed power. From this substantial data, a mapping of the overall double-pass amplifier performance can be derived for each PRF in terms of amplification efficiency, signal-to-noise ratio (e.g. ASE-suppression) and (critical) unabsorbed pump power. This representation also reveals a noticeable change of the optimum operation range between each fiber type (Fig. 2). Since lower seed powers make the fiber amplifier more sensitive to radiation-induced changes the interpretation is focused on the lowest PRF of 20 kHz.

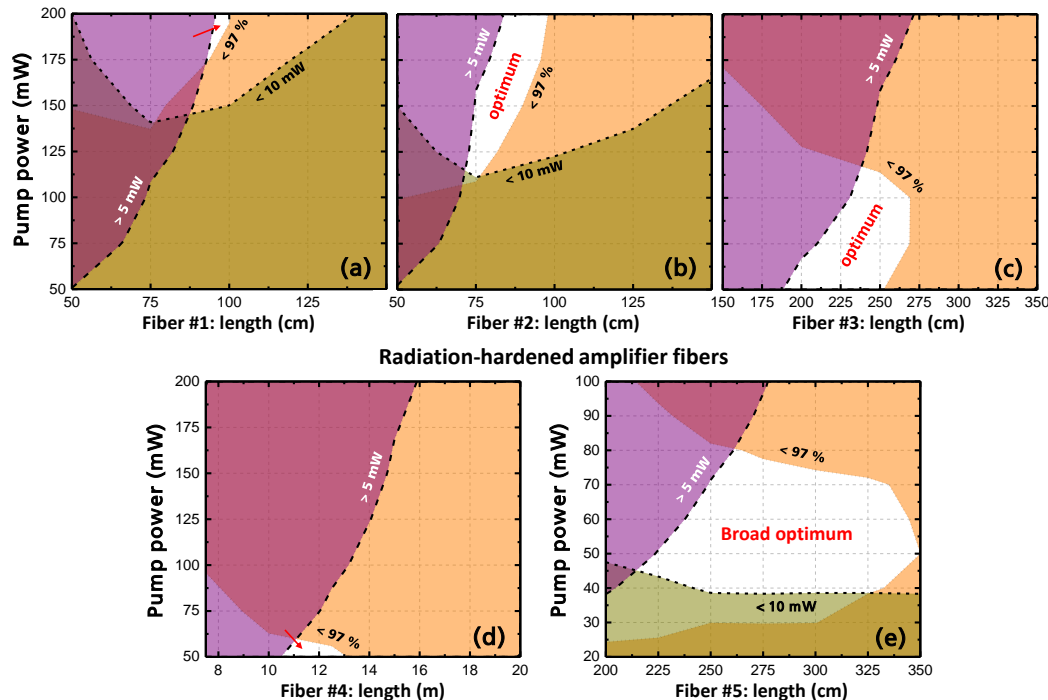


**Figure 2** Mapping of double-pass amplifier performance using five different fibers at lowest PRF (20 kHz). Within the white area, an optimum in terms of efficiency, signal-to-noise ratio and suppressed residual pump is reached (green area, average power <10 mW; violet area, residual pump power >5 mW; orange area, signal-to-noise ratio <97 %). Please note the different scaling of (e).

The signal-to-noise ratio is derived from the optical spectrum at OUT-1. The signal is defined as the spectral power within a 1-nm broad spectral window centered around the peak emission wavelength (1550 nm) whereas the noise comprises the remaining spectral power between 1500–1600 nm (Fig. 3). Reason for a deterioration of this parameter is mainly an increasing ASE-level as well as the impact of the nonlinear effect of degenerated four-wave-mixing (FWM) which preferably occur in longer fibers at anomalous dispersion wavelengths and

accordingly high peak powers. Due to its function as a first-stage high-gain pre-amplifier, an optimum performance is defined as: (A) average output power >10 mW at OUT-1 (gain >1600, >32 dB), (B) residual pump power <5 mW at OUT-2 and (C) signal-to-noise ratio >97 % at OUT-1.

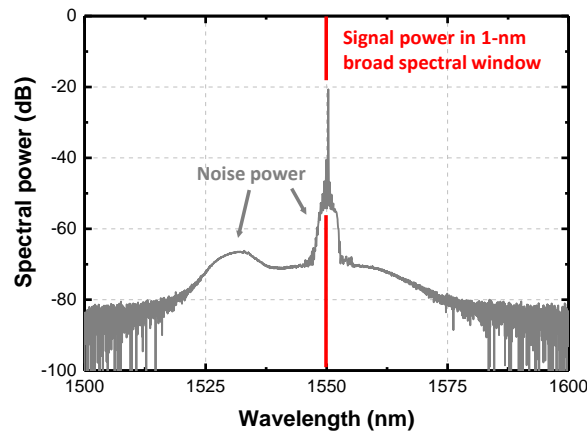


**Figure 3** Optical spectrum of fiber #5 set up in double-pass configuration measured at OUT-1 (PRF = 20 kHz, length = 275 cm, pump power = 60 mW). The signal-to-noise ratio is calculated from the signal (red) and the noise (grey) spectral components.

Fiber #1 has the largest core and the highest doping concentration of all tested fibers and is producing the results presented in Fig. 2a. Compared to fiber #2 (Fig. 2b), which has the same doping concentration but a smaller core, the performance optimum is reached only at significantly higher pump powers (110 mW vs. 175 mW). This indicates that the lower saturation power of the small-core amplifier fibers (see Figs. 2b–2e) is beneficial especially at low pulse repetition frequencies. Although the length of both fibers is conveniently short (high doping), the efficiency is comparatively low. This can be verified by analyzing fibers #3, #4 and #5 shown in Figs. 2c–2e, which exhibit lower doping concentrations and are exceeding the 10-mW output power boundary with less than 50 mW of 980-nm pump power at all PRF and chosen fiber lengths. As can be observed in Fig. 2d (fiber #4), with a low doping concentration (leading to 1530-nm peak absorptions of ~5 dB/m) the optimum fiber length is shifting well beyond 10 m. Passing twice this fiber length with concurrently sufficient amplification, FWM is generating new spectral components outside the signal wavelength leading to a decline of the signal-to-noise ratio. A balanced performance with a broad operating optimum is demonstrated by fiber #5, which features moderate doping (equivalent to a moderate fiber length), a small core-size as well as a radiation-hardened core-doping composition. From the presented experimental results two application-related design rules can be derived. Firstly, an optimum performance is reached at a 1530-nm peak core-absorption around 15 dB/m and, secondly, a smaller (4- $\mu$ m) core-diameter is preferable.

### III. SIMULATION: LASER PERFORMANCE DEPENDING ON RADIATION DOSE

The exposure of Erbium-doped fibers to ionizing radiation will induce background losses, which in turn reduce the laser performance. For this reason, the performance optimum is expected to be shifting. To predict the radiation dose dependent gain reduction, a complete model based on the rate equation under consideration of amplified spontaneous emission (ASE) has been set up, able to simulate the influence of radiation-induced absorption of the fiber on the amplifier performance [10,11]. The numerical analysis of the system was carried out under steady-state approximations, thus, no temporal saturation effects were included. Since the model does not combine rate equation with the nonlinear Schrödinger equation, the effect of four-wave mixing is currently withheld. For this reason, no signal-to-noise ratio is analyzed in our theoretical investigation.

Due to the rad-hard property and the balanced performance under experimental conditions described in section II, our investigation is focused on the performance alteration of fiber #5. Own measurements on Er-doped fibers during a constant exposure to the gamma radiation of a  $^{60}\text{Co}$  source had shown that the difference in radiation-induced absorption between 980-nm pump and 1550-nm signal wavelength equals a factor of 5.2. Based on this premise and a given background loss of 0.05 dB/krad at 1550 nm, the loss at pump wavelength will increase at a rate of 0.26 dB/krad accordingly. A seed power of 6.2  $\mu$ W is chosen, which represents the lowest repetition frequency of 20 kHz. To verify a realistic representation of the numerical results, model parameters were chosen to fit the measurements at best (Fig. 4).

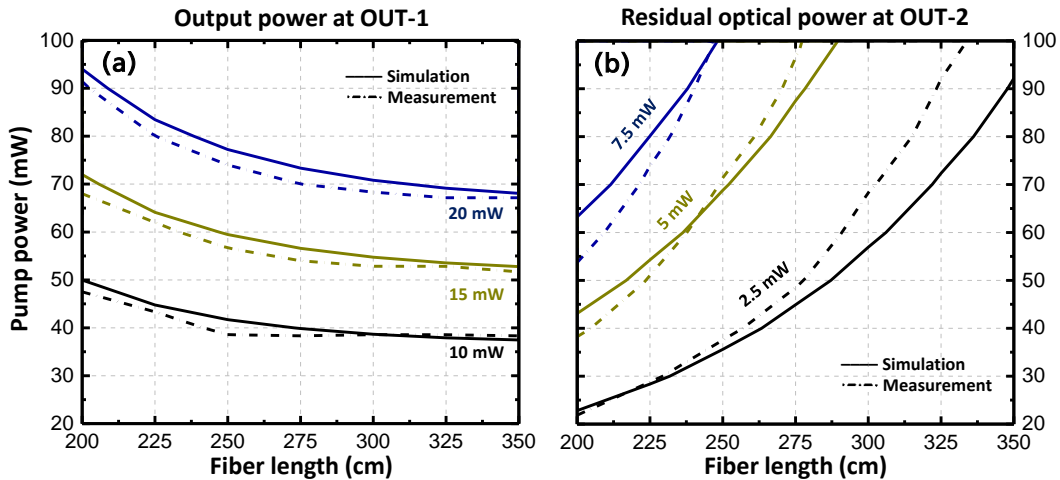


**Figure 4** Transformation of experimental data from Fig. 2e (solid line) into modelled data (dashed line) with (a) the output power at OUT-1 and (b) the residual optical light at OUT-2.

Differences between simulation and experiment in Fig. 4b can be attributed to the functional principle of the semiconductor-based power meter used for the measurement. Behind the fiber Bragg grating at OUT-2, the residual optical light is a blending of a small fraction of the 1550-nm signal pulse, continuous-wave ASE and continuous-wave 980-nm pump light. Since the InGaAs power meter response is wavelength and peak power sensitive, two different wavelengths and operation regimes cannot be measured accurately at the same time. Usually continuous-wave pump light is predominant, especially at higher pump powers and at shorter fiber lengths. But this assumption is not valid for the entirety of the investigated parameter field. On the other hand, the simulation is free from such restrictions. Thus, a reasonable trade-off is found by matching experimental data at fiber lengths <250 cm.

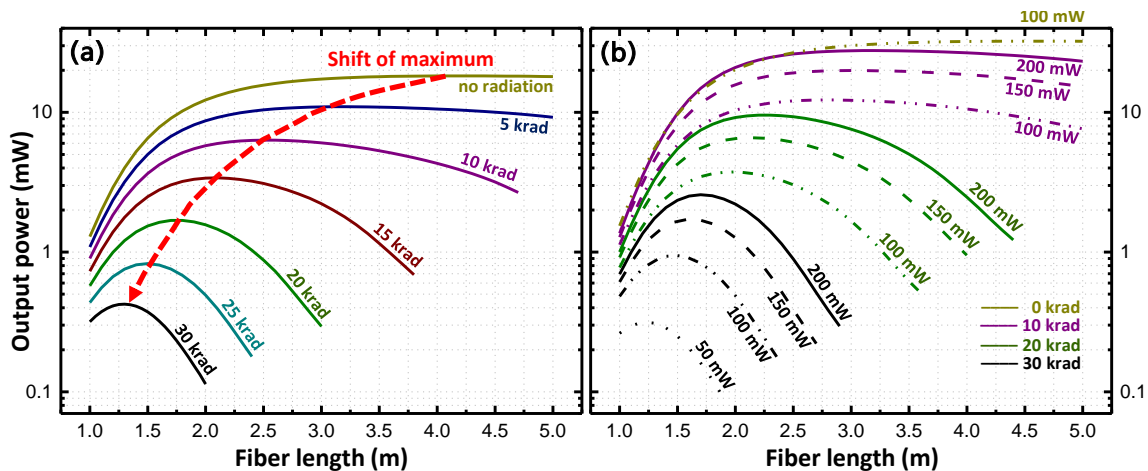


**Figure 5** Output power at OUT-1 for different radiation doses vs. fiber length at (a) constant pump power of 60 mW and (b) different pump powers which can partly compensate for radiation-induced gain losses.

Figure 5a shows the output power as a function of fiber length and total radiation dose. At approximately 20 krad, the maximum output power has dropped by 10 dB. In the process, the position of the maximum is shifting to a shorter fiber length too, e.g. from ~3.5 m (no radiation) to ~1.75 m (20 krad). As plotted in Fig. 5b, the radiation-induced gain loss can partly be compensated with a higher pump rate. For instance, the degradation from 10 to 20 krad of a 1.75 m long amplifier fiber can be counterbalanced by increasing the pump power from 100 to 200 mW.

The change of the dose-dependent optimum fiber length and its implication to output power and residual pump power is visualized in Fig. 6. At a constant pump power of 100 mW, the optimum fiber length is shifting from ~3.5 m to ~1.5 m along a nonlinear curve (Fig. 6a). With an increasing darkening of the fiber and due to the 5.2 times higher radiation-induced 980-nm pump light absorption, the issue of residual pump power is de facto vanishing even for relative short fibers as illustrated in Fig. 6b. Since the amplifier is starting its operation with a non-darkened fiber, the “no radiation” performance has always to be taken into account. Hence fiber length, pump power and accumulated end-of-life radiation dose have to be reconciled. E.g. if a constant

100 mW pump power is used (Fig. 6), the residual pump power will initially be  $>20$  mW for a fiber length of 1.5 m and it will not fall below 5 mW until 12.5 krad are accumulated. Using a constant current source to drive the pump laser diode does imply a longer fiber and/or less pump power. Based on the example of Fig. 6 (pump power = 100 mW) and on the assumption that the residual pump power must be kept below 5 mW, the optimum fiber length is  $\sim 2.8$  m. However, for high expected radiation levels short fiber lengths and higher pump powers are most favorable. A convenient means is the implementation of a pump power control, which can partly compensate for radiation-induced gain reduction and enabling the use of shorter fibers by reducing the pump power at the beginning and gradually adjusting the amplifier performance during mission.

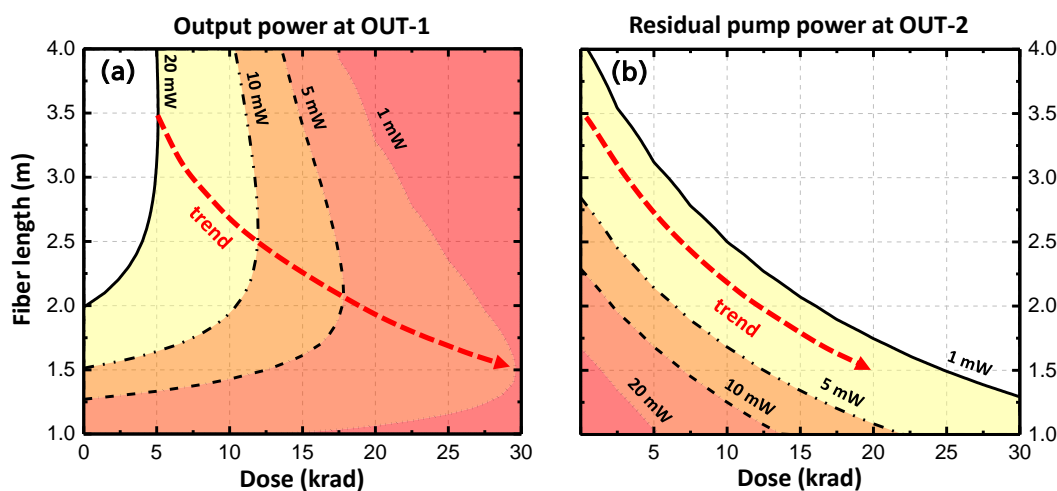


**Figure 6** Prognosticated trend of (a) output power at OUT-1 and (b) residual pump power at OUT-2 as a function of fiber length and radiation dose at a constant pump power of 100 mW.

#### IV. CONCLUSIONS

In conclusion, five different Er-doped single-clad fibers have been experimentally investigated in the same double-pass amplifier configuration, comparing different core-sizes, core-doping compositions and absorption characteristics in terms of amplifier efficiency, signal-to-noise ratio and critical unabsorbed pump power (section II). The performance was evaluated under different operation conditions generated by varying the parameters of fiber length and pump power at 20 kHz pulse repetition frequency. From this data, two application-related findings were derived, which indicate a generally favorable performance using 4- $\mu$ m core-diameter fibers with a moderate doping concentration (1530-nm absorption  $\sim 15$  dB/m). These tests inherently show equivalent compatibility of both the standard and the radiation-hardened amplifier fibers towards the passive fiber-optical components (FBG, WDM). In section III, the most promising fiber (#5) was further investigated by numerically analyzing the influence of radiation-induced absorption to the overall amplifier performance. As a result, a radiation-adapted redesign of the amplifier system, regarding pump power level and fiber length, can partly pre-compensate for the performance loss and allows for a balanced average performance over mission lifetime. Furthermore, this data can be used as seed input to estimate the performance of subsequent (fiber-) amplifier stages under the same radiation exposure. It should be noted, that the simulation does not include the implication of shielding and the compensating effect of photobleaching of radiation-induced color centers by 980-nm pumping [12]. Taking these issues into account, even higher radiation doses can be compensated by providing an adequate housing and/or allowing for photobleaching measures during flight.

#### ACKNOWLEDGEMENTS

The work presented was partly performed within the respective project by DLR German Space Agency under project no. 50 RA 1511 with funds from the German Ministry for Economy and Technology (BMBF) by enactment of the German Bundestag.

REFERENCES

- [1] Y. Jeong, S. Yoo, C. A. Codemard, J. Nilsson, J. K. Sahu, D. N. Payne, R. Horley, P. W. Turner, L. Hickey, A. Harker, M. Lovelady, and A. Piper, "Erbium:Ytterbium Codoped Large-Core Fiber Laser With 297-W Continuous-Wave Output Power," *IEEE Journal of Selected Topics in Quantum Electronics*, vol. 13, no. 3, May/June 2007.
- [2] L. Kotov, M. Likhachev, M. Bubnov, O. Medvedkov, D. Lipatov, A. Guryanov, K. Zaytsev, M. Jossent, and S. Février, "Millijoule pulse energy 100-nanosecond Er-doped fiber laser," *Optics Letters*, vol. 40, no. 7, April 2015.
- [3] E.-L. Lim, S. Alam, and D. J. Richardson, "High-energy, in-band pumped erbium doped fiber amplifiers," *Optics Express*, vol. 20, no. 17, pp 18803-18818, August 2012.
- [4] G. Sobon, D. Sliwinska, K. M. Abramski and P. Kaczmarek, "10 W singlemode Er/Yb codoped allfiber amplifier with suppressed Yb ASE," *Laser Phys. Lett.*, vol. 11, January 2014.
- [5] I. Pavlov, E. Dülgergil, E. Ilbey, and F. Ö. Ilday, "Diffraction-limited, 10-W, 5-ns, 100-kHz, all-fiber laser at 1.55  $\mu\text{m}$ ," *Optics Letters*, vol. 39, no. 9, pp 2695-2698, May 2014.
- [6] G. M. Williams, M. A. Putnam, C. G. Askins, M. E. Gingerich and E. J. Friebele, "Diffraction-limited, 10-W, 5-ns, 100-kHz, all-fiber laser at 1.55  $\mu\text{m}$ ," *Electronics Letters*, vol. 28, no. 19, pp 1816-1818, September 1992.
- [7] G. M. Williams, and E. J. Friebele, "Space Radiation Effects On Erbium-Doped Fiber Devices: Sources, Amplifiers, And Passive Measurements," *IEEE Transactions on Nuclear Science*, vol. 45, no. 3, pp 1531-1536, June 1998.
- [8] J. Thomas, M. Myara, L. Troussellier, E. Burov, A. Pastouret, D. Boivin, G. Mélin, O. Gilard, M. Sotom, and P. Signoret, "Radiation-resistant erbium-doped-nanoparticles optical fiber for space applications," *Optics Express*, vol. 20, no. 3, pp. 2435-2444, January 2012.
- [9] S. Girard, A. Laurent, E. Pinsard, T. Robin, B. Cadier, M. Boutillier, C. Marcandella, A. Boukenter, and Y. Ouerdane, "Radiation-hard erbium optical fiber and fiber amplifier for both low- and high-dose space missions," *Optics Letters*, vol. 39, no. 9, pp. 2541-2544, May 2014.
- [10] C. R. Giles, and E. Desurvire, "Modeling erbium-doped fiber amplifiers," *Journal of Lightwave Technology*, vol. 9, no. 2, pp. 271-283, February 1991.
- [11] [www.fiberdesk.com](http://www.fiberdesk.com).
- [12] K. V. Zotov, M. E. Likhachev, A. L. Tomashuk, A. F. Kosolapov, M. M. Bubnov, M. V. Yashkov, A. N. Guryanov, and E. M. Dianov, "Radiation Resistant Er-Doped Fibers: Optimization of Pump Wavelength," *IEEE Photonics Technology Letters*, vol. 20, no. 17, pp. 1476-1478, September 2008.